Monthly Notices
of the
ROYAL ASTRONOMICAL SOCIETY

MNRAS **464,** 104–113 (2017) doi:10.1093/mnras/stw2282

Doppler tomography and photometry of the cataclysmic variable 1RXS J064434.5+334451

J. V. Hernández Santisteban,[1,2]★ J. Echevarría,[2]★ R. Michel[3] and R. Costero[2]

[1]*Department of Physics & Astronomy, University of Southampton, Southampton SO17 1BJ*
[2]*Instituto de Astronomía, Universidad Nacional Autónoma de México, Apartado Postal 70-264, Ciudad Universitaria, México DF, CP 04510, México*
[3]*Instituto de Astronomía, Universidad Nacional Autónoma de México, Apartado Postal 877, Ensenada, Baja California, CP 22830, México*

Accepted 2016 September 8. Received 2016 September 7; in original form 2016 February 2

ABSTRACT

We have obtained simultaneous photometric and spectroscopic observations of the cataclysmic variable 1RXS J064434.5+334451. We have calibrated the spectra for slit losses using simultaneous photometry, allowing us to construct reliable Doppler images from Hα and He II 4686-Å emission lines. We have improved the ephemeris of the object based on new photometric eclipse timings, obtaining HJD = 245 3403.759 533 + 0.269 374 46E. Some eclipses present a clear internal structure, which we attribute to a central He II emission region surrounding the white dwarf, a finding supported by Doppler tomography. This indicates that the system has a large inclination angle $i = 78 \pm 2^{\circ}$. We have also analysed the radial velocity curve from the emission lines to measure its semi-amplitude, K_1, from Hα and He II 4686 and derive the masses of the components $M_1 = 0.82 \pm 0.06$ M$_{\odot}$, $M_2 = 0.78 \pm 0.04$ M$_{\odot}$ and their separation $a = 2.01 \pm 0.06$ R$_{\odot}$. The Doppler tomography and other observed features in this nova-like system strongly suggest that this is a SW Sex type system.

Key words: accretion, accretion discs – methods: observational – stars: individual: J0644+3344 – stars: individual: SW Sex – novae, cataclysmic variables.

1 INTRODUCTION

Cataclysmic variables (CVs) are semi-detached binary systems consisting of a white dwarf (WD) primary surrounded by a Keplerian disc accreted from a Roche-lobe-filling late-type secondary star. In systems where the mass transfer is high ($\dot{M} \sim 10^{-8}$ M$_{\odot}$ yr^{-1}, Townsley & Gänsicke 2009), the disc will become steady and remain bright for longer periods, suppressing the typical outbursts of CVs with lower mass transfer. These systems are commonly referred to as *nova-like variables* (NL). Thorstensen et al. (1991) constructed an initial qualitative description of NL systems that possess V-shaped eclipses, single-peaked lines and lags between the photometric and spectroscopic ephemeris, known as SW Sex stars. Recently, this list of properties was revised in order to account for an increasing variety of systems (including non-eclipsing) that share similar traits (Hoard et al. 2003).[1] Furthermore, SW Sex stars seem to be the dominant population of systems with orbital periods around 3–4 h (Rodríguez-Gil et al. 2007) and their possible connection to nova eruptions may provide information in the general context of CV evolution (Patterson et al. 2013).

1RXS J064434.5+334451 (hereinafter J0644) is a bright object ($V \sim 13.3$) discovered during the Northern Sky Variability Survey by Wozniak et al. (2004) (NSVS 7178256). It was initially identified as a β Lyrae object by Hoffman et al. (2008), but they point out that Sing et al. (2007) (hereinafter S07) have identified the object as a deep-eclipsing CV with an orbital period of nearly 6.5 h. The latter authors present the first spectroscopic and photometric study of this object and derive radial velocity semi-amplitudes for the primary and secondary stars, from which they obtain a mass ratio $q = 0.78$ and individual stellar masses in the range 0.63–0.69 M$_{\odot}$ for the white dwarf and 0.49–0.54 M$_{\odot}$ for the late-type star. They found that this NL resembles a UX UMa or SW Sex type object.

In this article, we present new spectroscopic and simultaneous photometry of J0644. We revisit the ephemeris of the system based on new observed eclipses, the shapes of which are discussed in detail. We discuss the radial velocity measurements of the Balmer Hα and high-excitation He II λ4686 emission lines. We present Doppler tomography reconstructions, calibrated with simultaneous photometry. Finally, a discussion is made regarding the classification of the object among CVs, which points towards the group of SW Sex type stars.

2 OBSERVATIONS AND REDUCTION

2.1 Spectroscopy

Time-resolved spectroscopy was performed at the Observatorio Astronómico Nacional at San Pedro Mártir, Mexico, on 2008

★ E-mail: j.v.hernandez@soton.ac.uk (JVHS); jer@astroscu.unam.mx (JE)

[1] See D. W. Hoard's Big List of SW Sextantis Stars at http://www.dwhoard.com/biglist.

© 2016 The Authors
Published by Oxford University Press on behalf of the Royal Astronomical Society

Downloaded from https://academic.oup.com/mnras/article-abstract/464/1/104/2194664 by University of St Andrews user on 10 September 2019

Table 1. Log of spectroscopic observations.

Date (UT)	HJD begin +245 4000	HJD end +245 4000	No. of images
Jan 09 2008	474.652 536	474.953 376	38
Jan 10 2008	475.650 633	475.944 017	35
Jan 11 2008	476.596 902	476.997 508	36
Jan 12 2008	477.648 375	477.838 742	23
Jan 13 2008	478.622 799	478.904 737	34
Jan 14 2008	479.627 510	479.711 502	12
Jan 15 2008	480.640 736	480.766 464	13

January 9–15. Observations were taken using the Echelle spectrograph and the SITe3 CCD detector at the $f/7.5$ Cassegrain focus of the 2.1-m telescope. Exposures of 600 s were used to obtain a resolution of $\phi \sim 0.025$ in orbital phase. The log of spectroscopic observations is presented in Table 1. We covered a full orbital period on most nights, except on January 12, 14 and 15, when we focused the observations around the primary eclipse. A Th–Ar calibration lamp was used every ten object images on average. The range in spectral coverage is λλ3980–7050 Å, with an average spectral resolution of $\simeq$20 km s^{-1}. Standard IRAF[2] procedures were used to reduce the data. No flux standard was observed, since we were focused on obtaining radial velocities from the data. Heliocentric corrections have been applied. In Fig. 1, we present the spectrum of J0644, which shows strong He I, He II and hydrogen Balmer lines in emission. Occasionally, we observe narrow absorption lines similar to those presented by S07.

2.2 Photometry

Differential photometry was also carried out at the Observatorio Astronómico Nacional at San Pedro Mártir, Mexico, in two seasons. All of the observations were made with the Thomson 2k CCD detector with a 3 × 3 binning at the 1.5-m Cassegrain telescope. During the first season, 2008 January 8–17, images were taken using 10-s exposures with the *V* filter. The second set of observations was performed during 2010 November 30–December 2. We used the same instrumental set-up as before for the first night and unfiltered images (white light, WL) with 3 s exposures for the last two nights. Standard data reduction was performed with IRAF's *apphot* routines. The images were corrected for bias and flat-field before aperture photometry was carried out. We calibrated the photometry with a star in the field, labelled as J0644–I by S07 with coordinates RA = 06$^{\rm h}$44′30.0″ and Dec. = +33°45′51″. The log of observations is presented in Table 2, where we have included observations by S07 used in our analysis (see Section 3). We will refer to each observation through the associated orbital cycle, *E*, of the primary eclipse.

3 PHOTOMETRIC ANALYSIS

3.1 TSA and PERIOD04 calculations

Our photometric data of J0644 were analysed for periodicities using the analysis of variance (AOV: Schwarzenberg-Czerny 1989; Devor 2005) included in the VARTOOLS suite (Hartman et al. 2008) and a discrete Fourier transform with PERIOD04 (Lenz & Breger 2005). Both methods show a clear peak at around 3.712 302 and 3.713 254 d^{-1} respectively, shown in Fig. 2. These values correspond to an orbital period $P \sim 6.46$ h, in good agreement with that reported by S07. Other peaks are present in the frequency analysis, but they appear to be main harmonics of the fundamental frequency Ω_1.

3.2 Primary eclipse and improved ephemeris

We fitted a Gaussian profile to every fully resolved eclipse and determined the time at mid-eclipse (see Fig. 3). These calculated times are shown in Table 2. A linear least-squares fit was then applied to the data using the orbital period and zero-phase point from S07 as initial parameters. Preliminary results showed that our ephemeris and those of S07 differ by 0.5 in phase. This was simply a confusion regarding the time of the inferior conjunction of the secondary. We consulted with the authors of S07 regarding this problem and they kindly provided us with their data for 2005 February and March observations (D. Sing, private communication). Their data are included in Table 2. We used their photometry in the *R* filter, which was also fitted using a Gaussian profile, to obtain their mid-eclipse points. These eclipse timings were consistent with our preliminary ephemeris; thus we have combined the data to obtain a larger time-based ephemeris:

$$HJD_{\rm mid\,eclipse} = 245\,3403.759\,533 + 0.269\,374\,46E,$$

where phase $\phi = 0.0$ is the inferior conjunction of the secondary star of the eclipsed source.

The errors are $\pm 1.8 \times 10^{-6}$ d for T_0 and $\pm 1.3 \times 10^{-7}$ d for the period. We see no evidence of a systemic variation in the O–C values, presented in Table 2. We should point out that our last eclipse (E7904) has such a complex shape that we did not take it into account in our calculations.

3.3 The 2008 photometry

Our main photometry results originate from the seven consecutive nights taken in 2008 shown in Fig. 4. We observed a small and gradual brightening of ∼0.4 mag towards the fourth night (12.8 mag) and a subsequent decline back to the initial 13.2 mag. The depth of the eclipse varies, with a maximum depth of 1.4 mag on the second night and a minimum of 1.2 mag on the fifth night. The two eclipses taken on the third night have almost the same depth. The eclipse on the fourth night was not observed fully, as the observations were interrupted around minimum light (see also Fig. 3, panel E3987).

3.4 Folded photometry

In Fig. 5, we show the 2008 photometric data folded in phase using our ephemeris. In general, the light curves show deep primary eclipses, as in the case of the *R* and *B* photometry by S07. Although some primary eclipses show a smooth drop in flux with a symmetric rise to the original flux level, others show a more complex shape. The eclipse shape can change from one cycle to the next, revealing a variable structure inside the primary eclipse. In these light curves, the variability is probably due to changes in the disc distribution brightness. An example of a non-symmetrical eclipse is night five (E3991; blue pentagons) where, around phase 0.99, we see small oscillations before minimum light. This was one of the nights when the object was brightest, with $V = 13.0$ mag outside eclipse.

This is not the only observed eclipse with an internal structure. In Fig. 6, we show an enhanced view of three asymmetrical eclipses

[2] IRAF is distributed by the National Optical Astronomy Observatories, which are operated by the Association of Universities for Research in Astronomy, Inc., under cooperative agreement with the National Science Foundation.

Downloaded from https://academic.oup.com/mnras/article-abstract/464/1/104/2194664 by University of St Andrews user on 10 September 2019

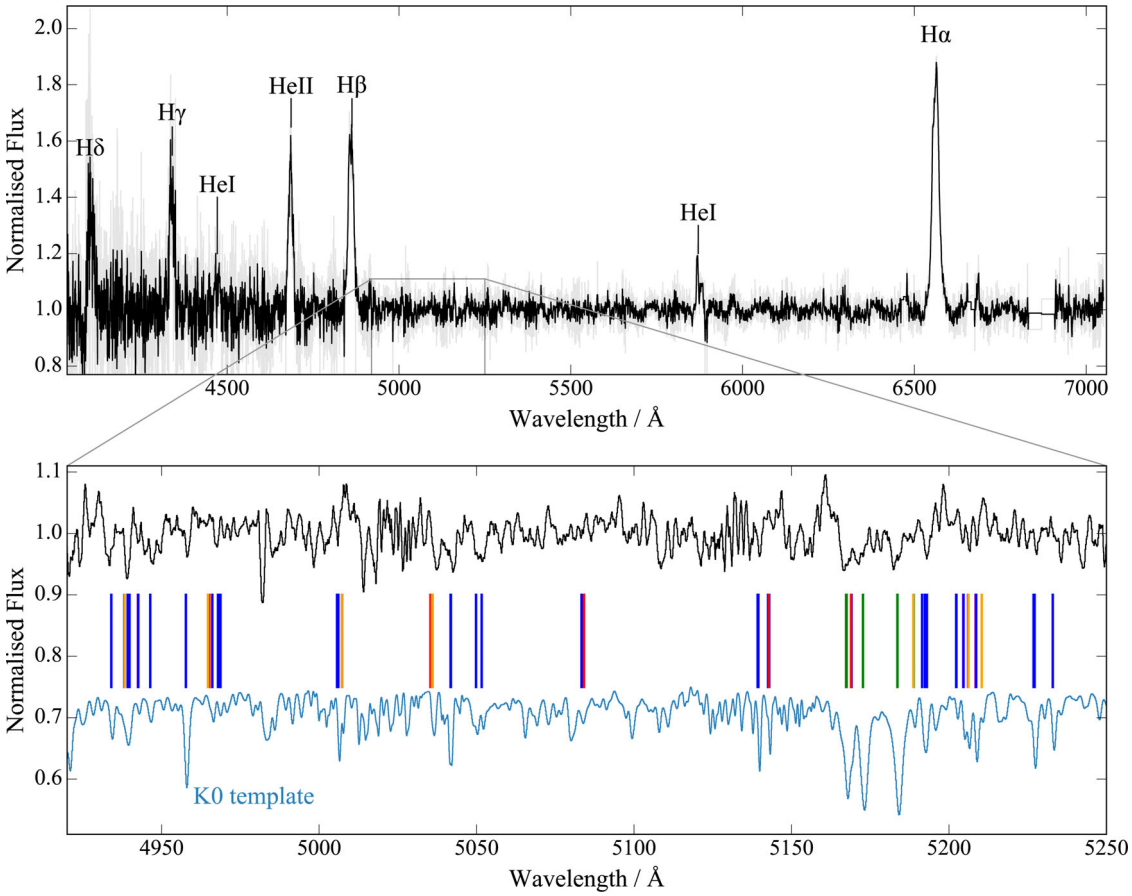

Figure 1. Average spectrum for J0644+3344 during the inferior conjunction of the secondary star. Top: we have added all the available spectra around phase 0.0 and normalized to the continuum. We have used a Savitzky–Golay filter with a 5-Å box to smooth the spectrum for clarity. Bottom: line identification of the donor features compared with a K0 template. We identify lines of Ca I (cyan), Cr I (purple), Fe I (blue), Mg I (green), Ni I (red) and Ti I (orange). Colours are displayed in the electronic version.

Table 2. Log of photometric observations.

Date (UT)	HJD begin +245 0000	HJD end +245 0000	No. of images	HJD mid-eclipse	Cycle[a] (*E*)	O–C (s)	Filter
Feb 02 2005[b]	3403.630 99	3403.869 02	300	3403.760 76	0	105.86	*R*
Feb 04 2005[b]	3405.617 62	3405.879 62	319	3405.645 18	7	2.15	*R*
Mar 01 2005[b]	3430.607 06	3430.760 33	107	3430.695 82	100	−100.23	*R*
Mar 02 2005[b]	3431.595 27	3431.799 32	111	3431.775 35	104	75.85	*R*
Jan 09 2008	4474.617 85	4474.954 18	1599	4474.7925	3976	13.64	*V*
Jan 10 2008	4475.608 21	4475.955 76	1541	4475.8702	3980	25.32	*V*
Jan 11 2008	4476.600 94	4477.004 59	1571	4476.6764	3983	−132.82	*V*
				4476.9482	3984	69.82	*V*
Jan 12 2008	4477.596 75	4477.908 55	1896	4477.7597	3987	129.84	*V*
Jan 13 2008	4478.623 64	4478.935 54	1912	4478.8345	3991	−132.8	*V*
Jan 14 2008	4479.606 03	4479.723 69	766	4479.6398	3994	−115.65	*V*
Jan 15 2008	4480.605 68	4480.798 76	937	4480.7177	3998	−73.73	*V*
Nov 30 2010	5530.922 31	5531.067 72	423	5531.0106	7897	−94.75	*V*
Dec 01 2010	5531.898 66	5531.992 92	765	···	7900	···	WL
Dec 02 2010	5532.822 11	5532.936 47	776	5532.8954	7904	8.17	WL

[a]Cycles *E* were calculated with the ephemeris presented in this article.
[b]Data by Sing et al. (2007).

plus one with no internal features. These are E3991 (blue pentagons), E7897 (red triangles) and the WL eclipse E7904 (green crosses). E3976 (black dots) is plotted as the reference of an almost featureless eclipse. The magnitudes of these light curves outside eclipse are in the range 13.0–13.2 mag. Several features should be noted in this graph. Between phases 0.91 and 0.97, the three asymmetric light curves show different behaviour, with a smoother decreasing shoulder. They also show a small hiatus around phase

Downloaded from https://academic.oup.com/mnras/article-abstract/464/1/104/2194664 by University of St Andrews user on 10 September 2019

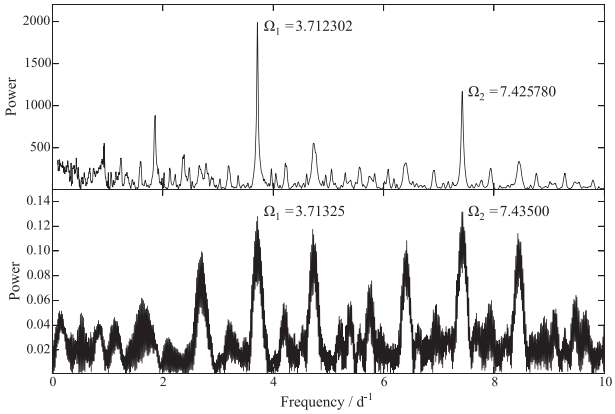

Figure 2. Time-series analysis periodograms for J0644+3344 photometry. Top: analysis of variance (AOV). Bottom: discrete Fourier transform. The frequency orbital period (Ω_1) and its first harmonic (Ω_2) are labelled.

0.98. E7897 shows a marked delay to minimum light, reaching 14.5 mag at phase 1.0 and close to the minimum value of E3976. On egress, E7897 also shows a clear feature at phase 1.04. The WL eclipse, E7904, shows a very complex structure. We observe a similar hiatus to E3991 and E7897 at phase 0.98, and then E7904 remains close to E3991 up to phase 1.02, after which it shows a second eclipse (shallower than the primary eclipse) with a minimum at phase 1.03. Thereafter, the brightness increases to reach a similar out-of-eclipse magnitude to E3991 and E7897. In general, these features could possibly be identified with the following: (a) the outside ingress of the WD+inner region (phase 0.94); (b) the inside ingress of the WD+inner region (phase 0.98); (c) the outside ingress of a hotspot (phase 0.99); (d) the inside ingress of a hotspot (phase 1.1); (e) the outside egress of the WD+inner region (phases 1.04–1.05). A close inspection of some of the S07 photometry also shows evidence of some of these features, even though they were taken with a smaller time resolution. Finally, E3991, E7897, E3983 and E3984 show a slanted bottom, indicating that, at times, some of the features in the accretion disc are totally occulted. This implies that the inclination angle is higher than the S07 estimate. This inclination can not be as high as 80°, since the evidence reviewed above indicates at most a grazing eclipse of the central emission surrounding the white dwarf by the secondary star. Furthermore, at such inclination angles we should see a definite secondary eclipse. For these reasons, we will use a conservative value of $i = 78 \pm 2°$, which includes the value used by S07 and includes the upper limit of 80°.

4 RADIAL VELOCITY ANALYSIS

Radial velocity measurements were performed for the hydrogen Balmer lines Hα and He II λ4686 Å. For the Balmer line, we used the standard double-Gaussian method with a diagnostic diagram developed by Shafter, Szkody & Thorstensen (1986) and a single Gaussian fit for the helium line. This method traces the emission of the wings of the line, presumably arising from the inner parts of the accretion disc; hence, it will follow the motion of the WD better. We adapted the IRAF *convrv* routine of the *rvsao* package modified by J. Thorstensen (2008, private communication) to perform a radial velocity fit to a circular orbit:

$$V(\phi) = \gamma + K_{\rm em} \sin(\phi - \Delta\phi), \quad (1)$$

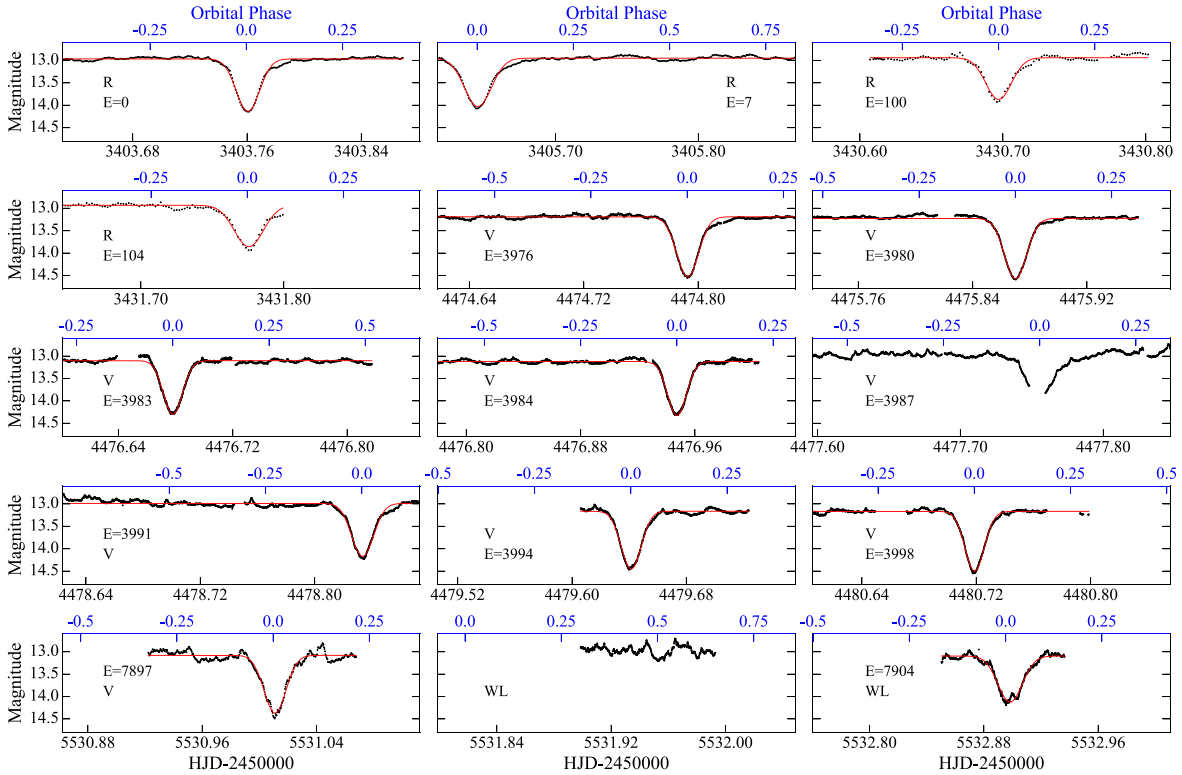

Figure 3. Differential photometry for J0644+3344. All axes are on the same time-scale, for comparison. The top axis (in blue) shows the orbital phase, centred at the corresponding epoch. The filter used on every light curve is indicated: R and V for Johnson *R* and *V*; WL for white light. Gaussian fits to each eclipse are marked by a continuous line (red in the electronic version). See text for details of each observation season.

Downloaded from https://academic.oup.com/mnras/article-abstract/464/1/104/2194664 by University of St Andrews user on 10 September 2019

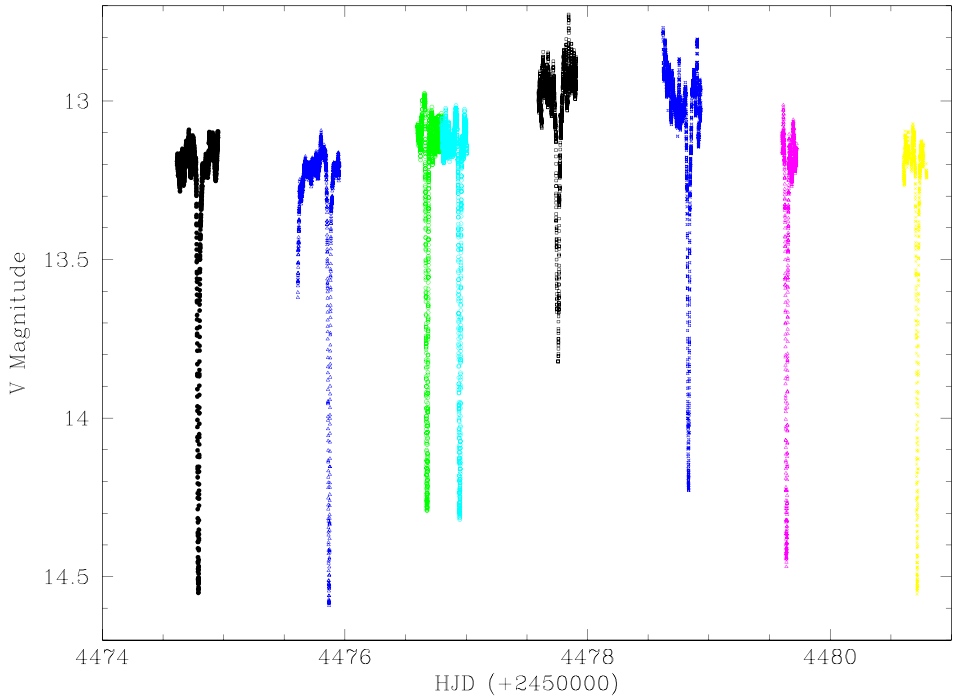

Figure 4. Johnson *V* photometry obtained in 2008 on seven consecutive nights. See text for details.

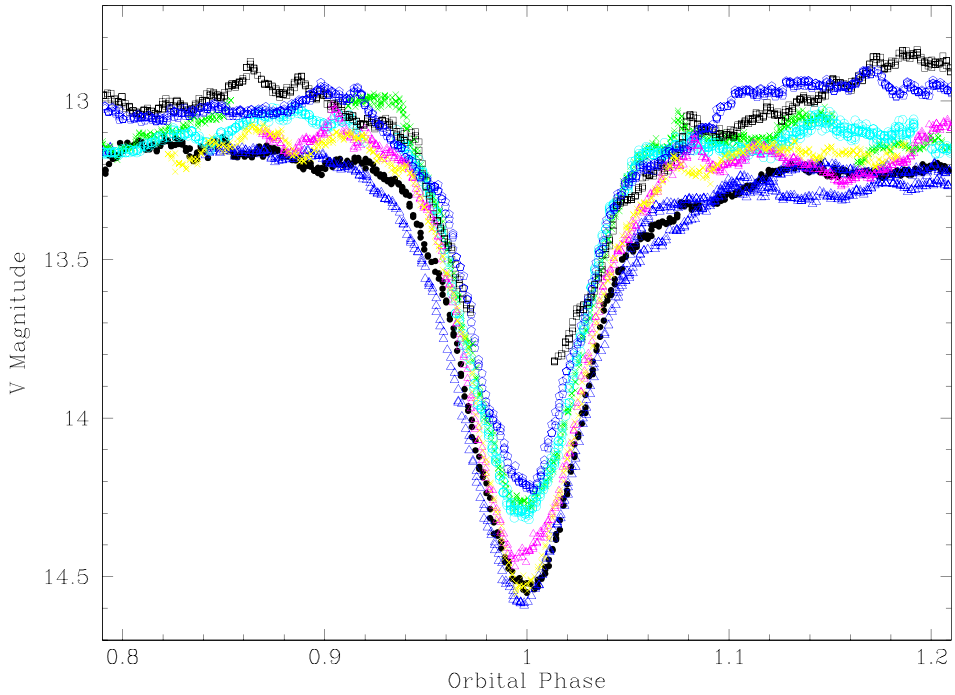

Figure 5. Detailed structure of the primary eclipses in 2008. The colours are the same as in Fig. 4 in the electronic version.

where γ is the systemic velocity, $K_{\rm em}$ is the semi-amplitude of the radial velocity curve and $\Delta\phi$ is the difference between the photometric and spectroscopic zero-points. We performed a grid search to find the optimal values for the Gaussian separation, α = 23–40 Å, and a width of ω = 9–13 Å, both in 0.1-Å steps. We evaluated each individual combination and used $\sigma(K)$ K^{-1} as the standard control parameter to find the minimum, e.g. Hα, shown in Fig. 7. We show the results of the analysis for Hα in the diagnostic diagram in Fig. 8. The $\sigma(K)$ K^{-1} indicator shows a clear minimum value for α = 29.9 Å.

Once the optimal radial velocities were found, we created 1000 bootstrap copies of the radial velocity curve and performed the fitting routine to obtain a robust uncertainty in the orbital parameters (Efron 1979). The distribution of parameter solutions is well described by Gaussians, which allowed us to retrieve the 1σ error of each parameter.

Downloaded from https://academic.oup.com/mnras/article-abstract/464/1/104/2194664 by University of St Andrews user on 10 September 2019

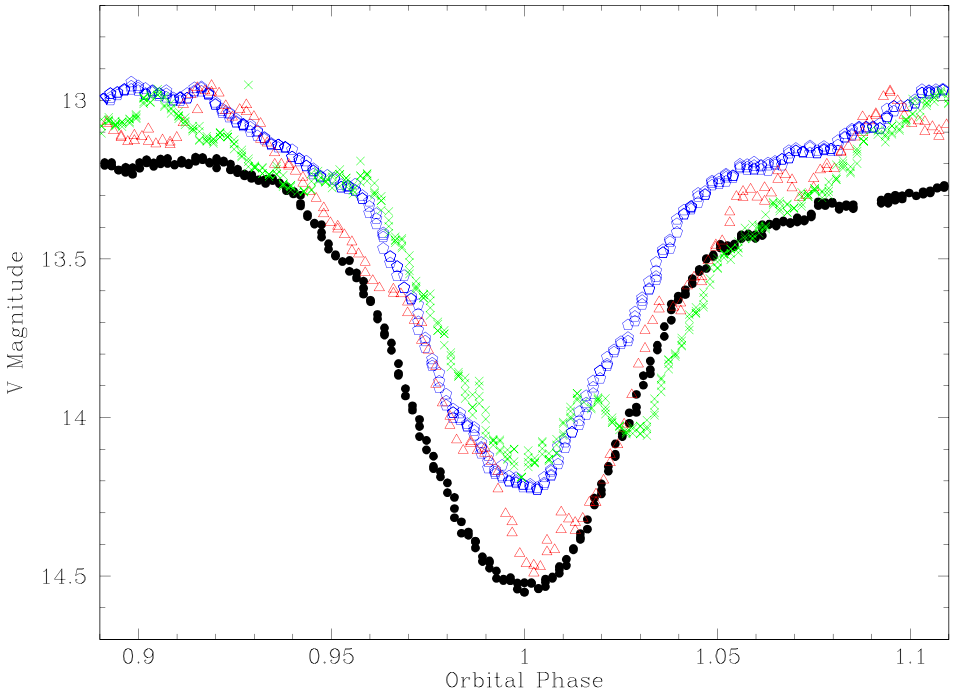

Figure 6. Enhanced view of four primary eclipses in 2008 and 2010. Symbols are as follows: E3991, blue pentagons; E7897, red triangles; E3976, black dots; E7904, green crosses. (Colours seen in the electronic version).

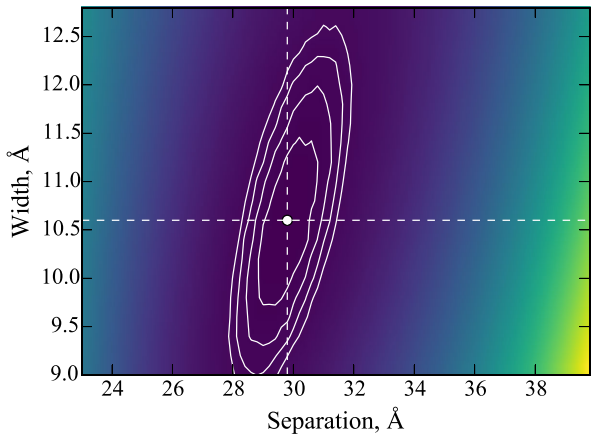

Figure 7. Two-dimensional map of the control parameter $\Delta\sigma K_1^{-1}$, used to select the best double Gaussian $\alpha = 29.8$ Å and $\omega = 10.6$ Å. Contours represent $\Delta\sigma K_1^{-1} = 0.001$.

The best solution for the radial velocities is shown in the top panel of Fig. 9. The solid curve correspond to the fits using the values presented in Table 3, where we show the parameter values obtained with the least-squares routine and the errors from the bootstrap technique. These errors have been scaled so $\chi^2_\nu = 1$. The optimal parameters are presented in Table 3.

The He II line is single-peaked throughout the full orbit. We performed a single Gaussian fit to every spectrum and obtained the corresponding radial velocities. We fitted equation (1) to the data and obtained the best parameters, shown in Table 3. Errors in the parameters were obtained via 1000 bootstrap copies in a similar way to that for Hα. The radial velocity curve is shown in the bottom panel of Fig. 9. These results are discussed in Section 7, where we compare the double-Gaussian method with the method used by S07.

5 THE DONOR STAR

S07 found the strongest evidence of the donor by performing cross-correlations with several standard stars with spectral types K3–K5. Although we see several weak absorption lines, most of these features are masked by the bright emission arising from the accretion disc during most of the orbit. Thus, we were unable the find a consistent solution to the radial velocities. We created an average spectrum around phase zero, where the absorption lines are most likely to be observed (see Fig. 1). The spectrum is consistent with a K0V star. The usual lines for spectral classification like Fe I λλ 4250, 4260, 4271 and Cr I lines λλ 4254, 4274, 4290, as well as Ca I λ 4226 (Gray & Corbally 2009), are too weak to be seen in this heavily masked spectrum, due to the presence of a strong blue continuum. We have therefore resorted to a direct comparison with the K0V star σ Draconis and compared the region 4900–5250, which is shown in the blow-out segment in the bottom panel of Fig. 1. It is well known that secondary stars in CVs tend to have larger radius than main-sequence stars for a given mass (Echevarría 1983; Beuermann et al. 1998; Knigge 2006). Therefore, obtaining mass from the spectral type or a mass–radius relation is not straightforward (the mass of a K0V is ∼0.89 $M_\odot$: Fernandes et al. 1998). Using empirically calibrated relations, we estimate a donor mass $M_2 = 0.85 \pm 0.22\ M_\odot$ (Knigge 2006; Knigge, Baraffe & Patterson 2011). However, this relationship is uncertain above 0.6 $M_\odot$, hence we favour the dynamical measurement of K_2 obtained by S07 in our mass estimate in Section 7. Nevertheless, both methods give similar results within the errors.

6 DOPPLER TOMOGRAPHY

Doppler tomography provides a method to obtain insight on the structure of the accretion disc, seen through a particular emission and/or absorption line (Marsh & Horne 1988). Tomograms are created in velocity space and careful interpretation is needed to infer

Downloaded from https://academic.oup.com/mnras/article-abstract/464/1/104/2194664 by University of St Andrews user on 10 September 2019

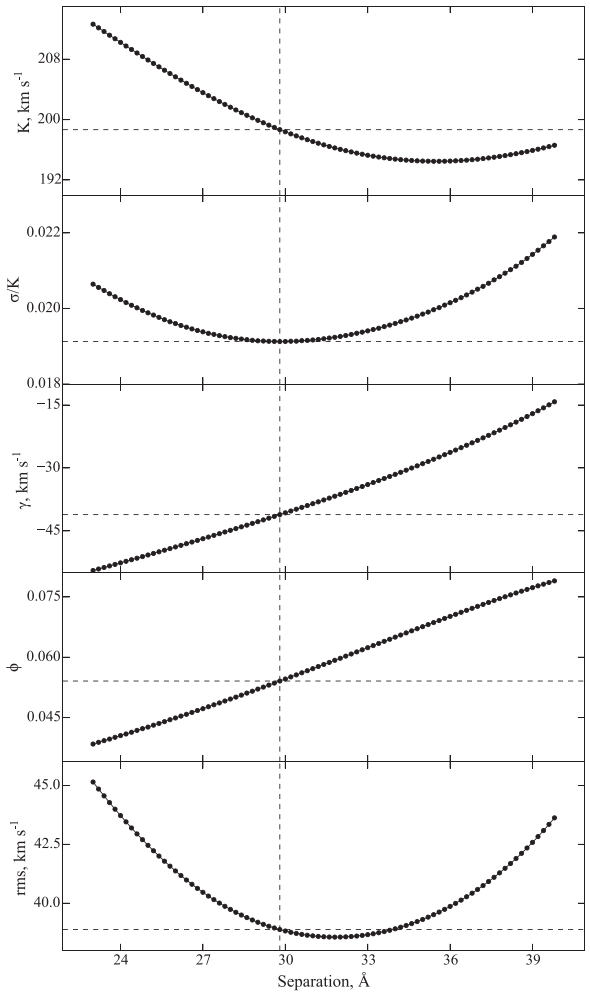

Figure 8. Diagnostic diagram for the Balmer Hα emission line. The parameters are shown as a function of the separation of the individual Gaussians. We used $\sigma(K)$ K^{-1} as the best solution parameter, which corresponds to a Gaussian separation of $\alpha = 29.8$ Å.

the physical position from where they are emitted. We used a code developed by Spruit (1998) based on the maximum entropy method.[3] We calibrated spectra using *V* Johnson simultaneous photometry to account for slit losses. Averaging of the simultaneous photometric data was performed, covering each spectroscopic exposure exactly and then summing all spectral fluxes centred at 5380 Å with a width of 98 Å. We then obtained a *V* Johnson-like flux (not convolved with the filter spectral response). The spectra were then calibrated accounting for the difference between photometric and spectroscopy magnitudes and correcting accordingly. Doppler maps were thus obtained for the emission lines Hα and He II 4686 Å (Fig. 10).

The Balmer Hα tomogram shows an emission region with a maximum at $(V_x, V_y) \simeq (+200,-300)$ km s^{-1} and a bright spot close to the secondary star (near the L1 point). In the higher contrast map (bottom row of Fig. 10), this spot appears connected with the larger region at negative V_y velocities. The Hβ tomogram (centre panels) presents a more extended emission region, ranging from $(-V_x, -V_y) = (-200, -700)$ km s^{-1} to $(-V_x, -V_y) = (500,0)$ km s^{-1}. The high

[3] http://www.mpa-garching.mpg.de/henk/pub/dopmap/

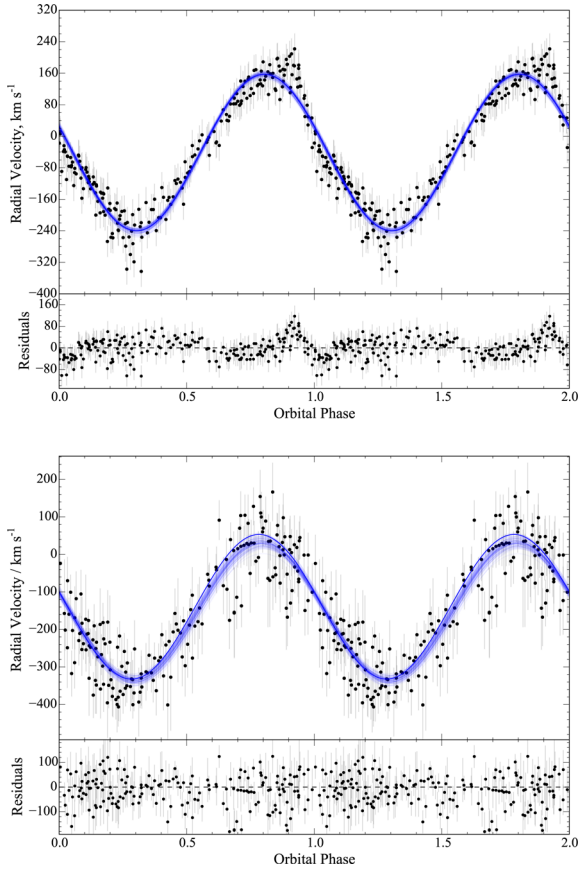

Figure 9. Radial velocity curves for (top) Hα and (bottom) He II λ4686 Å emission lines. The best solution is shown (blue lines), as well as random realizations via bootstrapping, to reflect the scatter of the solution. Errors in individual data points have been scaled so that $\chi^2_\nu = 1$.

Table 3. Radial velocity solutions for the emission lines in J0644.

Line	K_1 km s^{-1}	γ km s^{-1}	$\phi - \phi_{\rm phot}$
Hα	198 ± 4	−41 ± 3	0.05 ± 0.01
He II λ4686	184 ± 8	−150 ± 6	−0.04 ± 0.01

excitation line He II λ4686 (right panels) is seen in the tomogram as a single blob of material around or close to the WD centred at $(V_x, V_y) = (+0,-200)$ km s^{-1}. These tomograms are consistent with previous studies on NL-type systems (Kaitchuck et al. 1994; Neustroev et al. 2011).

At phase $\phi = 0.0$, the Balmer lines are visible even though the system undergoes deep eclipses. A minimum is found at phase 0.125 (consistent with the tomography), and in fact shows a double peak throughout phase 0.375 as different parts of the large emission is occulted. In general, the Balmer lines present a complex but similar behaviour during the full cycle. The blueshifted peak in both lines is more intense throughout phase 0.0–0.25, probably due to the strength shown in the tomography in the negative V_x part of the elongated emission. There is a clear double peak at Hα present at phases 0.375 and 0.75, phases at which we would expect to see the hotspot near the secondary more clearly and separated from the blob in its less elongated position. We must stress that the high-excitation He II λ4686 Å is always present as a single peak at all phases, although weaker near phase zero. The He II line shows a

Downloaded from https://academic.oup.com/mnras/article-abstract/464/1/104/2194664 by University of St Andrews user on 10 September 2019

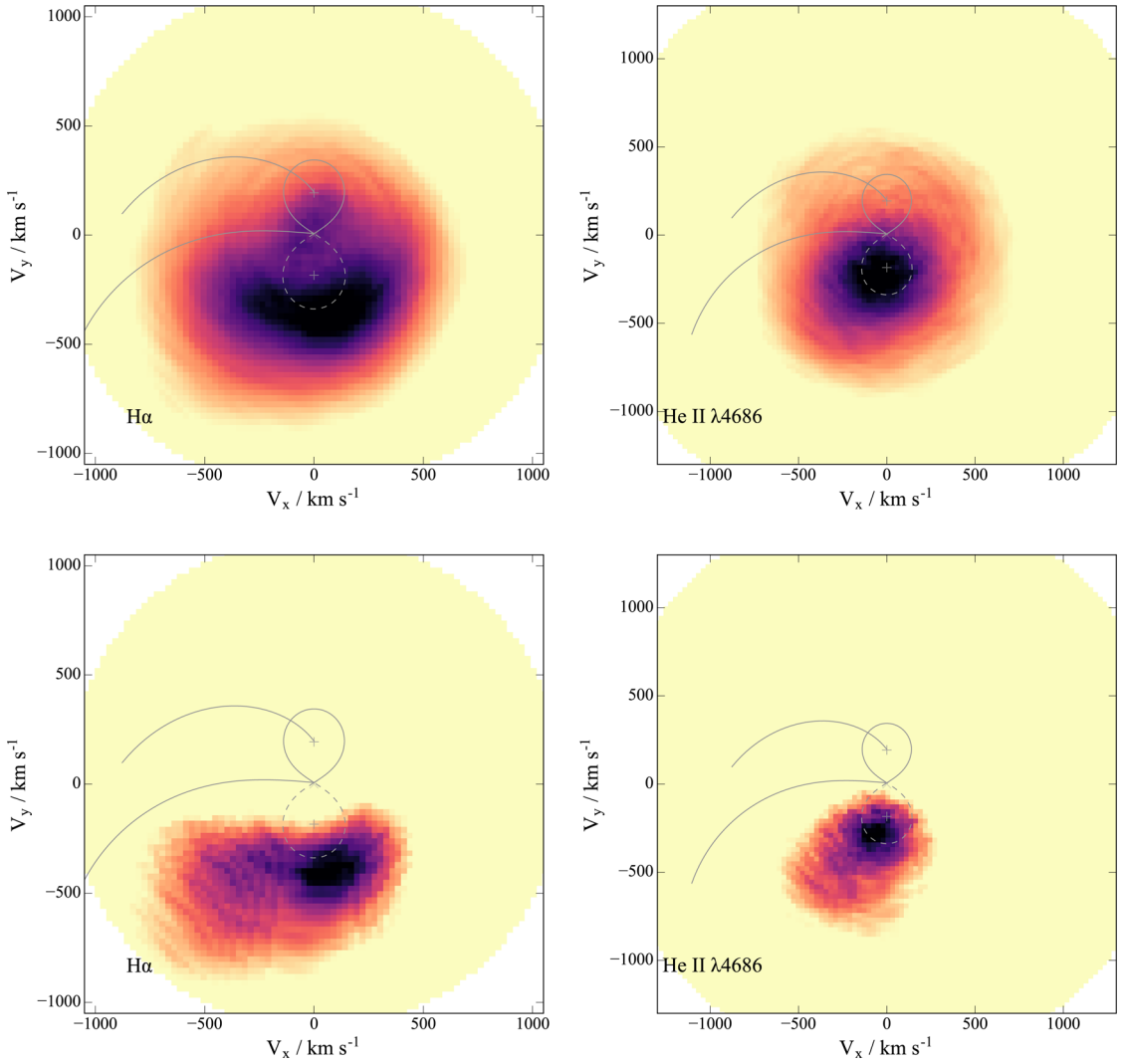

Figure 10. Doppler tomography of J0644 for (left) Hα and (right) He II λ4686-Å emission lines. The Roche lobe surface was calculated using the orbital parameters discussed in this article: $i = 78^{\circ}$, $q = 0.96$ and $\gamma = -7.1$ km s^{-1}. The Keplerian and ballistic trajectories in the upper figures are marked as the upper and lower curves, respectively. The crosses are the velocity (from top to bottom) of the secondary star, the centre of mass and the primary star. (See text for discussion.) The bottom figures show the same tomograms after subtracting an azimuthal average to highlight the asymmetric emission components.

minimum at phases 0.0–0.125, but does not disappear completely. This suggests that the blob we are looking at in the tomogram may surround the central WD completely and may arise from outside the orbital plane, but this could also be the result of seeing the extended weaker emission shown in the lower right tomogram of Fig. 10.

7 DISCUSSION

Accurate masses of CVs are difficult to obtain, even in eclipsing systems, since it is rarely possible to look directly at the WD. Instead, we rely on the radial velocity curve of the emission lines arising from the accretion disc, which can possess asymmetries that may lead to inaccurate results. Furthermore, the surface of the secondary star could be irradiated and the measurements from its absorption lines could give an out of centre-of-mass radial velocity semi-amplitude. These problems have been discussed in full by Warner (1995), although modern studies with high-resolution spectroscopy have proven useful in deconvolving these asymmetries, as in the case of U Gem (Echevarría, de la Fuente & Costero 2007).

Our radial velocity analysis of J0644 clearly indicates that the disc has large asymmetries, as shown in the Balmer line. This is consistent with the findings by S07, particularly with their results for the He I λ4471 line in absorption (see their fig. 9). Our Doppler tomography shows that the Balmer emission comes from a large, but asymmetric region located on the far side of the accretion disc with respect to the secondary. We must point out, however, that our observations do not show the strong central absorption in the H I and He I lines observed by S07. We must therefore assume that the accretion disc was in a different state. However, the He II tells us another story. While S07 ascribe the bulk of the He II emission as coming from inside the inner disc, our Doppler tomography results indicate that the He II emission arises from a concentrated region around the white dwarf. Nevertheless, these two interpretations should not affect the $K_{\rm He\,II}$ value. The S07 results for the He II line give $K_{\rm He\,II} = 151 \pm 5$ km s^{-1}, compared with our results of $K_{\rm He\,II} = 184 \pm 8$ km s^{-1}. We highlight the strong difference between our Fig. 9 and fig. 11 of S07. In both cases, the positive radial velocities reach a maximum of about 100 km s^{-1}. However, our maximum negative velocities reach about -350 km s^{-1}, while

Downloaded from https://academic.oup.com/mnras/article-abstract/464/1/104/2194664 by University of St Andrews user on 10 September 2019

in S07 they go no further than -250 km s^{-1}. S07 measured the centre of wavelength from each line profile to calculate the Doppler velocity of H I, He I and He II lines. They found, in general, that the radial velocity curve from these lines (in absorption and emission) presents a flat bottom from phases 0.0–0.5, which they attribute to line blending, magnetic effects, non-uniform disc emission or effects from an accretion stream. They also claim that He II in emission is exempt from this non-sinusoidal behaviour. This may not be so. Although the solid line in their fig. 11 is a sinusoidal, this may be misleading, as the radial velocity measurements do seem to be affected by this flattening behaviour between phases 0.1 and 0.4. The cause of this effect may be simply the way in which their individual spectra were measured. The centre-of-wavelength approach may result in distorted radial velocities. This method may not be the cause per se. It is possible that the asymmetric bulk may play a role in this distortion in both H I and He I lines, when, at these phases, the bulk is behind the white dwarf. However, it is also possible that we have observed the system at a different accretion stage and the flattening may be due to a stronger distortion in both H I and He I lines. This possibility is supported by the fact that we do not observe strong central absorption in the H I line. We must also point out that our H I radial velocity curve does not suffer from this flattening effect. If anything, we observe an excess of negative radial velocities at phase 0.25. If our arguments are correct, then our He II radial velocity should reflect the motion of the white dwarf more accurately. This value is also supported by our Doppler tomography (see Section 6), which indicates that that the centroid of the velocity He II blob has a velocity around $\sim$200 km s^{-1}.

S07 estimates a semi-amplitude of the secondary of $K_2 = 192.8 \pm 5.6$ km s^{-1}. We will use the latter in our estimates of the orbital parameters. Therefore, we can establish an independent mass ratio of $q = K_1/K_2 = 0.96 \pm 0.05$. We adopted our improved orbital period, $P_{\rm orb} = 0.26937446$ d, to estimate the mass functions:

$$M_1 \sin^3 i = \frac{P K_2 (K_1 + K_2)^2}{2\pi G} = 0.77 \pm 0.06\,{\rm M}_\odot,$$

$$M_2 \sin^3 i = \frac{P K_1 (K_1 + K_2)^2}{2\pi G} = 0.73 \pm 0.07\,{\rm M}_\odot$$

and

$$a \sin i = \frac{P(K_1 + K_2)}{2\pi} = 2.01 \pm 0.05\,{\rm R}_\odot.$$

Assuming an inclination angle of $i = 78 \pm 2^\circ$, the system parameters are

$$M_1 = 0.82 \pm 0.06\,{\rm M}_\odot,$$

$$M_2 = 0.78 \pm 0.07\,{\rm M}_\odot,$$

$$a = 2.05 \pm 0.06\,{\rm R}_\odot,$$

where the errors reflect both the masses and inclination angle uncertainties. At these high inclination angles, the error produced by uncertainties is small and the results are dominated largely by the error in the masses and the separation of the binary.

Our results yield larger masses for both the primary and secondary stars (within the uncertainties) than the upper limits given by S07. The separation of the binary is also slightly larger than that estimated by S07. However, these purely dynamical measurements provide a mass of the WD in line with the average mass of CVs (Zorotovic, Schreiber & Gänsicke 2011). The mass of the donor is in agreement with the expected value from semi-empirical evolutionary sequences (Knigge et al. 2011), as calculated in Section 5.

7.1 Narrow absorption spectra

Although we detected narrow absorption features mainly in the Balmer lines, around phase 0.5, we were unable to reproduce the results of S07, due to a lack of appropriate spectra. S07 used two spectra taken at phases -0.0788 and -0.0177 and subtracted them, with the purpose of discovering whether the spectrum of the WD reveals itself. What they found is a spectrum (see their fig. 11) with strong narrow absorption lines of H I, He I, Mg II and Ca I, instead of the broad features expected from a white dwarf. They concluded that the region producing this spectrum could arise from a region containing the WD and an inner accretion disc or could be the result of some newly formed pre-WD. Our Doppler tomography of Hα and He II λ4686 Å suggests that this absorption spectrum is the result of accretion stream overflow (i.e. the disc regions detected through the Balmer lines) seen at large optical depths against the bright inner regions around the WD (e.g. Hellier & Robinson 1994). This supports the explanation by S07 that we are looking at a region with deep H I and He I absorption lines, with a blackbody temperature of about 25 000 K.

7.2 An SW Sextantis system?

J0644 exhibits most of the characteristics of an SW Sex type star, as defined originally by Thorstensen et al. (1991) and Hoard et al. (2003). It is a nova-like CV showing deep primary eclipses and a high inclination system. It displays high-excitation lines, including He II λ 4686 Å. It shows single-peak emission lines, instead of the double-peaked emission expected from near-edge-on discs. It shows shallower Balmer lines during the primary eclipse and also transient absorption lines around phase 0.5. Two characteristics of SW Sex stars do not comply for J0644. It has an orbital period way outside the 3–4 h criterion and it does not exhibit pronounced radial velocity phase offsets with respect to phase zero, as defined by the eclipses. There are now several newfound CVs with large orbital periods, like BT Mon, V363 Aur, AC Cnc and LS Peg, definitely confirmed as SW Sex systems, plus a number of possible candidates. Therefore, this last criterion might be only a selection effect, as only the criterion of having just an eclipsing system should apply in order to belong to this group. Our Doppler tomography shows that the Balmer lines are produced in J0644 by elongated and strong emission, located opposite the secondary star with respect to the centre of mass of the binary. This is similar to the Doppler tomography found in BH Lyn (Dhillon et al. 1992). A small phase shift could be produced if the main emitted material is located opposite the secondary star. Another case that shows concentrated emission in different parts of the disc is the case of BF Eri (Neustroev & Zharikov 2008), which also shows a small phase lag.

8 CONCLUSIONS

We have improved the ephemeris of the object through differential photometry. A slow and short brightening of $\sim$0.4 mag was observed in 2008. Our radial velocity analysis allowed us to obtain values for the semi-amplitudes of both components of the system. Doppler tomography revealed that the He II emission arises from the WD and provides a good indicator of its radial velocity semi-amplitude. From our adopted values for K_1, K_2 and $i = 78 \pm 2^\circ$, we find $M_1 = 0.82 \pm 0.06$ M$_\odot$, $M_2 = 0.78 \pm 0.04$ M$_\odot$ and a separation

Downloaded from https://academic.oup.com/mnras/article-abstract/464/1/104/2194664 by University of St Andrews user on 10 September 2019

of the binary $a = 2.05 \pm 0.06$ $R_{\odot}$. We found that the general characteristics of J0644 are consistent with a SW Sex nova-like CV. Follow-up observations, especially simultaneous spectroscopy and photometry, are needed to understand the nature of this object better.

ACKNOWLEDGEMENTS

The authors are indebted to DGAPA (Universidad Nacional Autónoma de México) support, PAPIIT projects IN111713 and IN122409. JVHS acknowledges financial support from CONACyT (Mexico) scholarship programmes, the MSc programme at IA-UNAM and the University of Southampton. The authors thank all staff at the OAN for their invaluable help. This research has made use of NASA's Astrophysics Data System. We thank the anonymous referee for a prompt response and excellent feedback.

REFERENCES

Beuermann K., Baraffe I., Kolb U., Weichhold M., 1998, A&A, 339, 518
Devor J., 2005, ApJ, 628, 411
Dhillon V. S., Jones D. H. P., Marsh T. R., Smith R. C., 1992, MNRAS, 258, 225
Echevarría J., 1983, Rev. Mex. Astron. Astrofis., 8, 109
Echevarría J., de la Fuente E., Costero R., 2007, AJ, 134, 262
Efron B., 1979. Ann. Statist., 7, 1
Fernandes J., Lebreton Y., Baglin A., Morel P., 1998, A&A, 338, 464
Gray R. O. C., Corbally J., 2009, Stellar Spectral Classification
Hartman J. D., Gaudi B. S., Holman M. J., McLeod B. A., Stanek K. Z., Barranco J. A., Pinsonneault M. H., Kalirai J. S., 2008, ApJ, 675, 1254
Hellier C., Robinson E. L., 1994, ApJ, 431, L107
Hoard D. W., Szkody P., Froning C. S., Long K. S., Knigge C., 2003, AJ, 126, 2473
Hoffman D. I., Harrison T. E., Coughlin J. L. McNamara B. J., Holtzman J. A., Taylor G. E., Vestrand W. T., 2008, AJ, 136, 1067
Kaitchuck R. H., Schlegel E. M., Honeycutt R. K., Horne K., Marsh T. R., White J. C. II., Mansperger C. S., 1994, ApJS, 93, 519
Knigge C., 2006, MNRAS, 373, 484
Knigge C., Baraffe I., Patterson J., 2011, ApJ, 194, 28
Lenz P., Breger M., 2005, Commun. Asteroseismol., 146, 53
Marsh T. R., Horne K., 1988, MNRAS, 235, 269
Neustroev V. V., Zharikov S., 2008, MNRAS, 386, 1366
Neustroev V. V., Suleimanov V. F., Borisov N. V., Belyakov K. V., Shearer A., 2011, MNRAS, 410, 963
Patterson J. et al., 2013, MNRAS, 434, 1902
Rodríguez-Gil P. et al., 2007, MNRAS, 377, 1747
Schwarzenberg-Czerny A., 1989, MNRAS, 241, 153
Shafter A. W., Szkody P., Thorstensen J. R., 1986, ApJ, 308, 765
Sing D. K., Green E. M., Howell S. B., Holberg J. B., Lopez-Morales M., Shaw J. S., Schmidt G. D., 2007, A&A, 474, 951
Spruit H. C., 1998, preprint (arXiv:astro-ph/9806141)
Thorstensen J. R., Ringwald F. A., Wade R. A., Schmidt G. D., Norsworthy J. E., 1991, AJ, 102, 272
Townsley D. M., Gänsicke B. T., 2009, ApJ, 693, 1007
WarnerB., 1995, Cataclysmic Variable Stars. Cambridge Univ. Press, Cambridge
Wozniak P. R. et al., 2004, AJ, 127, 2436
Zorotovic M., Schreiber M. R., Gänsicke B. T., 2011, A&A, 536, A42, doi:10.1051/0004-6361/201116626

This paper has been typeset from a TEX/LATEX file prepared by the author.

Downloaded from https://academic.oup.com/mnras/article-abstract/464/1/104/2194664 by University of St Andrews user on 10 September 2019